Collapsing cavities, toroidal bubbles and jet impact

By J. R. Blake, M. C. Hooton, P. B. Robinson and R. P. Tong

School of Mathematics and Statistics, The University of Birmingham, Edgbaston, Birmingham B15 2TT, UK

The present study is aimed at clarifying some of the factors which affect the formation and direction of a liquid jet in a collapsing cavity and the pressures induced on a nearby rigid boundary. The flow can be accurately represented by a velocity potential leading to the use of boundary integral methods to compute bubble collapse. For configurations with axial symmetry, the jet motion and that of the bubble centroid are along the axis of symmetry. Examples are presented for bubbles close to a rigid surface and to a free surface. These are followed through to the toroidal stage after jet penetration. When there is no axis of symmetry, fully three-dimensional computations show that the buoyancy force can cause the jet to move parallel to a vertical rigid boundary, thus negating its damaging effect. The computational study is extended to model cavitation bubble growth and collapse phases in a forward stagnation point flow as a model of reattachment of a boundary layer; a region where severe cavitation damage is often observed. The Kelvin impulse is introduced to aid a better understanding of the mechanics of bubble migration and jet direction in the examples presented. Finally a comparison between the spherical and axisymmetric theories is made for an oscillating bubble in a periodic pressure field; this being of particular interest to current studies in acoustic cavitation and sonoluminescence.

1. Introduction

One of the main mechanisms for damage to hydraulic structures by cavitation, or to naval structures by an underwater explosion, is the violent collapse phase of the bubble. A high speed liquid jet often penetrates the bubble and its impact can induce a large pressure loading on a nearby structure. However, in the case of cavitation, only a small number of bubbles present in the flow are responsible for damage to a surface, while for an underwater explosion the damage caused is also difficult to predict.

The size of bubbles considered in the present study ranges from as little as 10 μm in radius for some cavitation bubbles, to 10 m and more for underwater explosions. For the purposes of experimental observation bubble sizes of 2–3 cm in a reduced pressure environment are often generated (Blake & Gibson 1981, 1987). The period of bubble oscillation varies from microseconds to seconds; for example, an underwater explosion with a maximum bubble radius of 10 m has a period of the order of one second. The fluid motions associated with these rapid bubble oscillations (surface velocities can be as large as 10^3 m s^{-1}) generate very large pressures in the surrounding fluid, from 10^2–10^3 times atmospheric pressure. In addition shock waves are common when the

Phil. Trans. R. Soc. Lond. A (1997) **355**, 537–550
Printed in Great Britain

TEX Paper

bubble volume is a minimum (either at its inception, or at the end of each oscillation period) and these can give rise to short-lived pressures greater than 10^3 atm. Forcing of bubble oscillations by an ultra-sound device can produce temperatures in the bubble contents from order 10^2 K to estimated values of 10^6 K (Crum 1995; Moss *et al.* 1994). The study of bubble dynamics thus provides many examples of extreme free surface motions.

The present paper is organized into the following sections. Section 2 outlines the results of numerical simulations using the boundary integral method for both axisymmetric and fully three-dimensional geometries. Section 3 examines the behaviour of a cavitation bubble in a stagnation point flow, modelling the reattachment of a boundary layer. An analytic framework is provided for the numerical and experimental results in § 4 by the Kelvin impulse theory, § 5 reports on the excitation of bubble motion by an acoustic field, while § 6 places the current study in perspective with regard to realistic, practical problems in transient bubble dynamics.

2. Boundary integral methods

For many transient bubble motions the viscosity of the liquid (commonly water) and the effect of surface tension are negligible. In these cases the liquid can be considered to be ideal and irrotational so that its motion is described by a velocity potential $\phi(\boldsymbol{x}, t)$ which satisfies Laplace's equation in the liquid. With these assumptions, the boundary integral method provides an efficient means of computing the evolution of a bubble surface in time, including the interaction of a bubble with a rigid boundary or a free surface. The solution procedure involves only a discretization of the boundaries, $\partial\Omega$, of a fluid domain Ω. Given the initial conditions of the position of any free surfaces and rigid boundaries, together with the values of ϕ on the free surfaces and $\partial\phi/\partial n$ on the rigid boundaries, Laplace's equation is solved in integral form as

$$\tfrac{1}{2}\phi(\boldsymbol{p}) = \int_{\partial\Omega} \left(\frac{\partial\phi}{\partial n}(\boldsymbol{q}) G(\boldsymbol{p}, \boldsymbol{q}) - \phi(\boldsymbol{q}) \frac{\partial G}{\partial n}(\boldsymbol{p}, \boldsymbol{q}) \right) \mathrm{d}\Omega_q, \tag{2.1}$$

to give $\partial\phi/\partial n$ on the free surfaces, where $\boldsymbol{p}, \boldsymbol{q} \in \partial\Omega$, assumed smooth and

$$G(\boldsymbol{p}, \boldsymbol{q}) = 1/(4\pi|\boldsymbol{p} - \boldsymbol{q}|).$$

The normal direction is taken to be outward (i.e. into the bubble). This leads to the construction of the free surface velocities which are used to advance these surfaces forward in time by means of the kinematic and dynamic boundary conditions

$$\frac{\mathrm{d}\boldsymbol{x}}{\mathrm{d}t} = \nabla\phi, \quad \boldsymbol{x} \in S_\mathrm{b}, \tag{2.2}$$

$$\frac{\mathrm{d}\phi}{\mathrm{d}t} = \frac{1}{2}|\nabla\phi|^2 - \alpha \left(\frac{V_0}{V} \right)^\lambda - \delta^2(z - z_0) + \frac{\kappa}{We} + 1, \tag{2.3}$$

where S_b is the bubble surface. Here, $\mathrm{d}/\mathrm{d}t$ denotes the material derivative and Cartesian coordinates are chosen such that gravity acts in the negative z-direction.

Non-dimensional parameters are used with length scaled with respect to the maximum bubble radius R_m, time with respect to $R_\mathrm{m}(\rho/\Delta p)^{1/2}$. The pressure scale is $\Delta p = p_\infty - p_\mathrm{c}$ and p_c is the liquid vapour pressure (taken to be constant), with p_∞ the hydrostatic pressure at the depth of bubble inception, z_0. In the case of two

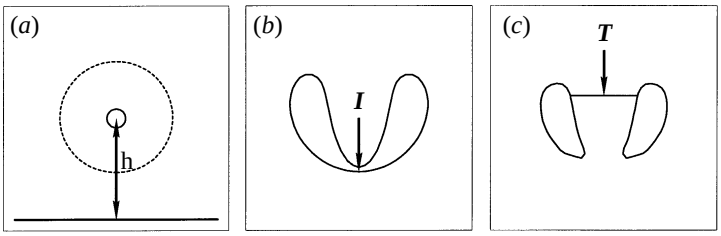

Figure 1. (*a*) The location of the point of bubble inception. (*b*) A cut is introduced at the point of impact, I, in order to continue to the toroidal phase. (*c*) An arbitrary cut, T, is introduced at each time step for the toroidal bubble.

bubbles, R_{m} is taken to be the maxium radius attained by the larger bubble. Expansion or compression of any non-condensible gas inside the bubble is assumed to be adiabatic and λ is the ratio of specific heats, with V the bubble volume and V_0 the initial volume at $t = 0$. Surface tension effects can be included and κ is the sum of the principal curvatures of the bubble surface. For an infinite free surface bounding the fluid domain, the pressure is taken to be constant on this surface and is set to zero. The significant dimensionless parameters are the bubble standoff from any rigid boundary (γ), buoyancy (δ), the pressure due to any non-condensible contents of the bubble (α) and the Weber number (We), with

$$\gamma = \frac{h}{R_{\mathrm{m}}}, \quad \delta = \left(\frac{\rho g R_{\mathrm{m}}}{\Delta p}\right)^{1/2}, \quad \alpha = \frac{p_0}{\Delta p}, \quad We = \frac{R_{\mathrm{m}} \Delta p}{\sigma},$$

where σ is the surface tension, h is the distance of the point of bubble inception from the nearest rigid boundary (see figure 1*a*) and p_0 is the initial pressure due to any non-condensible bubble contents.

Information on aspects of the computation relating to the numerical methods associated with solving (2.1) can be found in Blake *et al.* (1986, 1987), Oğuz & Prosperetti (1990) and Best (1993). In some cases it was necessary to smooth the surface shape by exploiting the formula developed by Longuet-Higgins & Cokelet (1976) in connection with their study of water waves.

In figure 2 calculations based on the axisymmetric version of the code are illustrated for a cavitation bubble near a rigid boundary (figure 2*a*), a free surface (figure 2*b*) and for two bubbles near either a rigid boundary (figure 2*c*), or a free surface (figure 2*d*). Figure 2*a* shows the particle paths of a number of particles from initiation until 'touchdown' of the high speed liquid jet. It is of particular interest to note the near parallel particle pathlines of the jet. In figure 2*b* it can be observed that the liquid jet is directed away from the free surface (in contrast to the rigid boundary where the jet is directed towards the boundary). The other notable feature is the free surface 'spike' which moves vertically at a near constant velocity. Longuet-Higgins (1983) has analysed the local flow near the tip as a Dirichlet hyperboloid, obtaining 'spike' velocities in excellent agreement with the experimental studies reported in Blake & Gibson (1981). In figure 2*c* it is observed that the lower bubble collapses from the side. The upper bubble plays the role of an 'image bubble,' thus creating an effective rigid wall, hence the collapse from the side as if it is located in a channel between two plates (see, for example, Chahine 1982). In figure 2*d* the lower bubble does not influence the upper bubble significantly.

After jet impact a toroidal bubble is formed and the liquid domain is no longer simply connected. Connectivity of the computational domain is restored by means

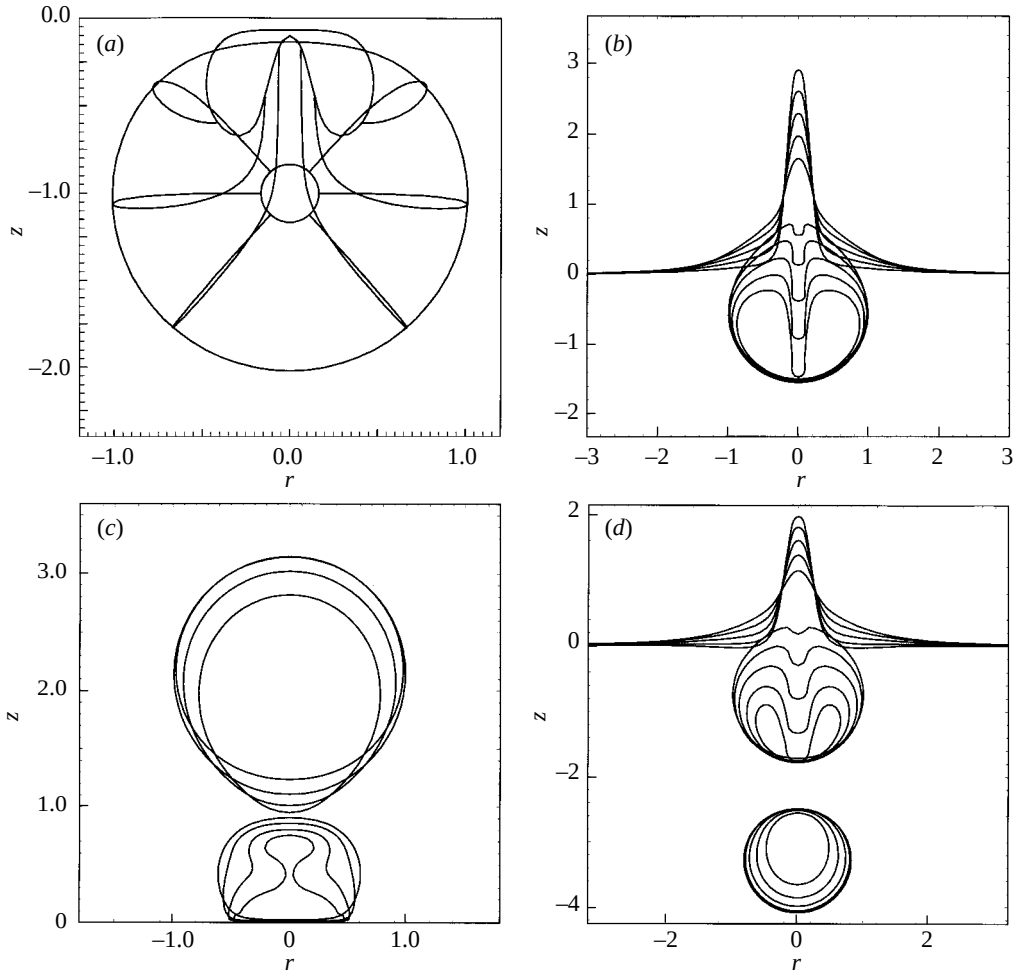

Figure 2. Vapour bubbles, $\alpha = 0$. (*a*) The particle paths during growth and collapse for a bubble below a rigid boundary, $\gamma = 1.0$, $\delta = 0$. (*b*) The collapse of a single bubble near a free surface. (*c*) The collapse of two different sized bubbles above a rigid boundary. (*d*) The collapse of two bubbles beneath a free surface.

of a cut (see figure 1*b*, *c*) and the integral equation now includes an additional term:

$$\tfrac{1}{2}\phi(\boldsymbol{p}) = \int_{\partial\Omega} \left(\frac{\partial\phi}{\partial n}(\boldsymbol{q}) G(\boldsymbol{p},\boldsymbol{q}) - \phi(\boldsymbol{q}) \frac{\partial G}{\partial n}(\boldsymbol{p},\boldsymbol{q}) \right) \mathrm{d}\Omega_q - \Delta\phi \int_T \left(\frac{\partial G}{\partial n_+}(\boldsymbol{p},\boldsymbol{q}) \right) \mathrm{d}\Omega_q. \tag{2.4}$$

Integration over T, the surface of the cut, takes account of any circulation introduced at the jet impact by allowing a jump in ϕ values, with $\Delta\phi = \phi_+ - \phi_-$ where the subscripts $\pm$ identify the upper and lower sides of T. A detailed theoretical analysis of the jet impact process is given in Best (1993). The central concept of the theory depends on impact at a point with no resulting generation of a vortex sheet. This is consistent with the original mathematical model which does not allow any energy loss, since there is no mechanism for this in the model. A later approach by Zhang *et al.* (1993) extends the approach of Best to incorporate a vortex sheet.

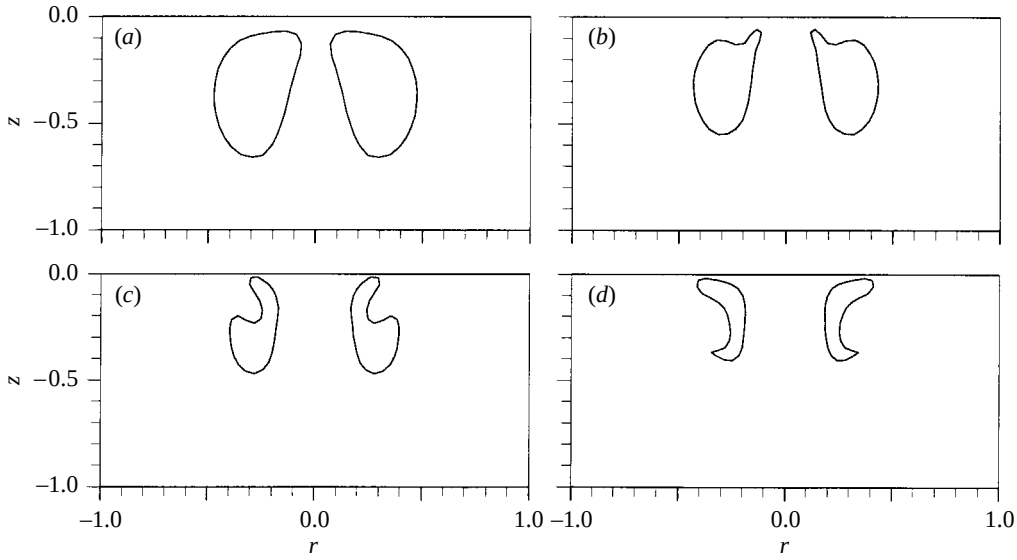

Figure 3. The formation of a toroidal bubble after jet impact for $\gamma = 1.0$.

Figure 3 shows the development of the toroidal bubble for $\gamma = 1$ and times 2.26 through to 2.43. Figure 4*a* plots the centreline pressures as a function of time for this case. Two high local peak pressures are predicted, the earlier one associated with jet impact, while the marginally later one coincides with the large internal pressures inside the bubble at minimum volume. However, this picture is incomplete, since if we examine figure 4*b*, it is observed that while the peak pressure at the instant of jet impact is on the centreline there are higher pressures off-axis. These are a combination of the pressures associated with the bubble minimum volume and the high speed lateral fluid motion which yields the characteristic 'slamming' pressures. Recent calculations by King & Needham (1994) suggest that the boundary integral code will need to be modified to take account of the singular behaviour of the potential during this part of the impact process.

The discussion to date has concentrated on the simpler axisymmetric studies. However, the practical problems that have motivated these studies (cavitation and underwater explosions) require a comprehensive three-dimensional study, for which computational details are given in Blake *et al.* (1995). In figure 5, the role of buoyancy is explored by increasing the parameter δ. It is clear that buoyancy can mitigate the Bjerknes boundary attraction for larger values of δ, causing the jet to move in a more vertical direction.

3. Stagnation point flow

The flow over an elongated body is relevant to applications in hydraulic machinery. The stagnation zone associated with the reattachment of a separated flow is identified by Knapp (1955) as the location of the most severe cavitation damage on the body surface. However, Knapp estimates that only one bubble in 30 000 is likely to cause damage. Bubble inception occurs in the low pressure region near the blunt nose of the body and bubbles are swept over the separated region to the higher pressure region near reattachment, where they collapse causing large fluid velocities and high

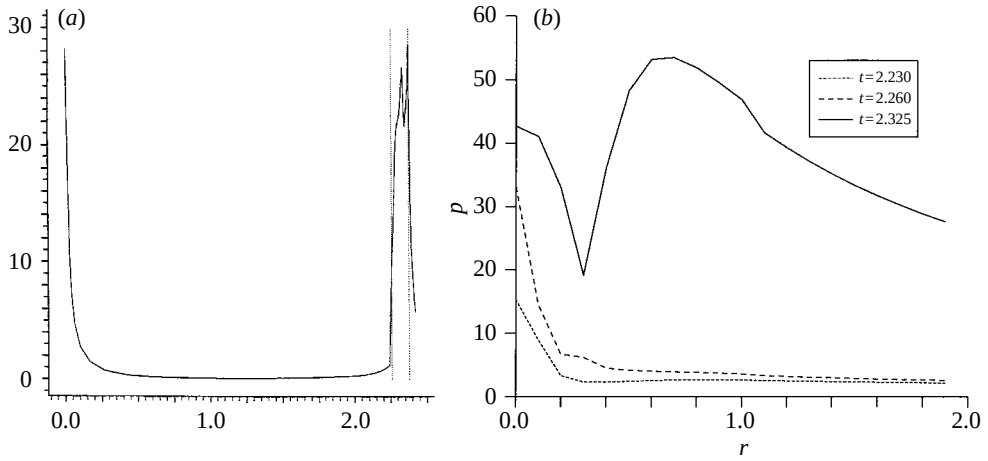

Figure 4. Non-dimensional pressure at the rigid boundary during bubble collapse: (*a*) on the axis of symmetry (pressure against time), the vertical broken lines show the time of jet impact followed by the time of minimum volume; (*b*) along the boundary (pressure against radial distance).

pressures. This results in noise as well as damage to the nearby boundaries due to a number of factors which include collective bubble phenomena, shocks and high speed liquid jets impacting directly onto the boundary (see, for example, Brennen 1995). To investigate this last aspect, Starrett (1982) conducted a series of experiments on the collapse of cavitation bubbles in an axisymmetric stagnation point flow. The parameters of these experiments are used to provide initial conditions for the present theoretical results.

An ideal stagnation point flow along the z-axis is assumed, defined by the velocity potential

$$\phi_s = \tfrac{1}{4}\beta\left(x^2 + y^2 - 2z^2\right). \tag{3.1}$$

By introducing a modified velocity potential

$$\phi(\boldsymbol{x}, t) = \phi_b(\boldsymbol{x}, t) + \phi_s(\boldsymbol{x}), \tag{3.2}$$

the boundary integral formulation already described can be introduced to solve for ϕ_b, the perturbation to the stagnation point flow caused by the bubble. The pressure scale now becomes,

$$\Delta p = p_\mathrm{u} - p_\mathrm{c}, \tag{3.3}$$

where, p_u is the pressure in the undisturbed flow at the point of bubble inception,

$$p_\mathrm{u} = p_\mathrm{s} - \tfrac{1}{2}\beta^2\gamma^2, \tag{3.4}$$

with p_s, the pressure at the stagnation point.

As defined earlier, γ is the non-dimensional distance of the inception point of the bubble from the stagnation point on the rigid boundary. This gives, for a cavitation bubble in the absence of gravity and ignoring surface tension effects, the dynamic boundary condition on the bubble surface,

$$\frac{\mathrm{d}\phi}{\mathrm{d}t} = \tfrac{1}{2}|\nabla\phi|^2 + \tfrac{1}{2}\beta^2\gamma^2 + 1. \tag{3.5}$$

An approximate initial condition is used to start the computation by adding to the stagnation flow potential that due to a Rayleigh bubble of small radius.

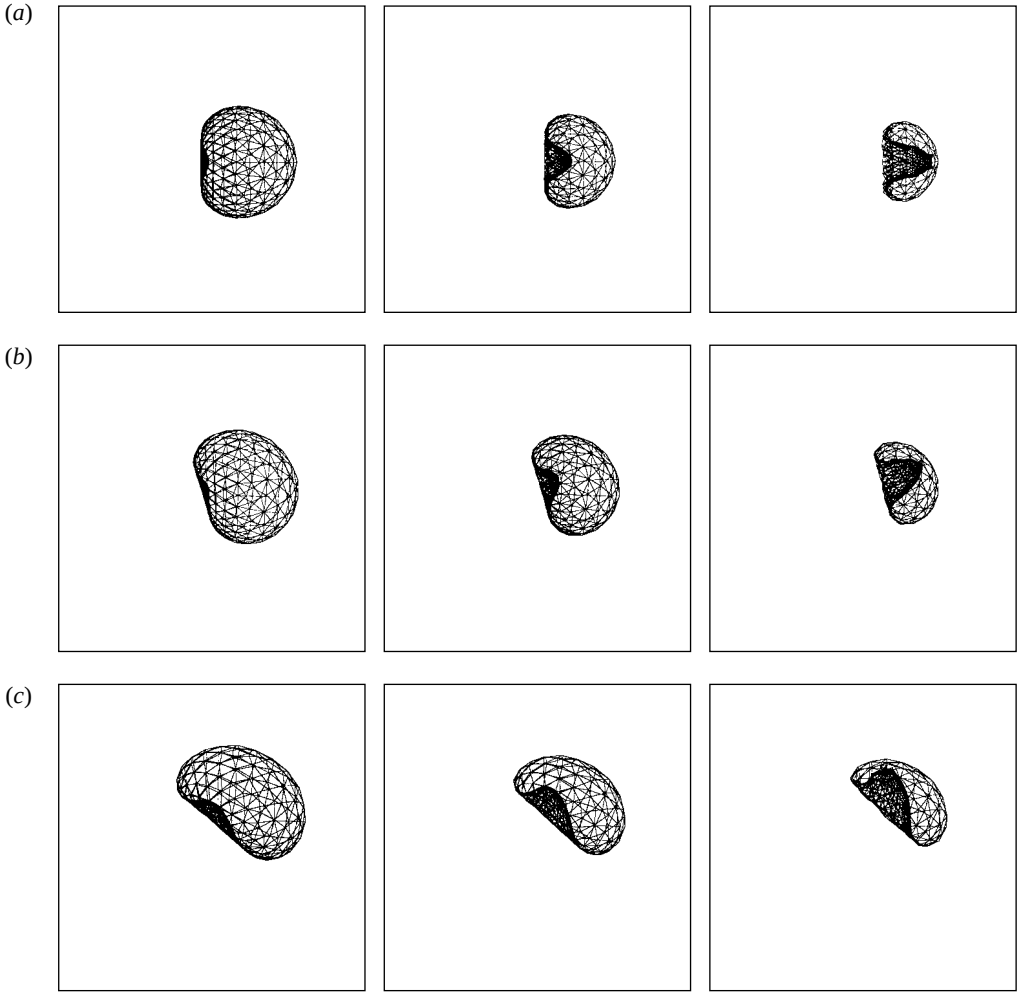

Figure 5. The expansion and collapse of an explosion bubble near a vertical wall for $\gamma = 2.0$, showing the effect of increasing the buoyancy parameter δ: (*a*) $\delta = 0$; (*b*) $\delta = 0.1$; (*c*) $\delta = 0.2$.

In figure 6*a* computational results are shown for the collapse phase of an example from Starrett's experiments corresponding to a free stream velocity of $6.9\ \mathrm{m\,s^{-1}}$. It is observed that a circumferential jet develops in this case leading to the formation of two bubbles and two ultrafine high speed jets. The continuation of this type of collapse is illustrated in figure 6*b* for the case of an initially perturbed bubble. It is unlikely that these ultrafine jets would be damaging to the rigid boundary. However, in figure 6*c*, a slower stagnation flow is used resulting in a small 'hump' appearing at the top of the bubble, which leads to an extremely fast, fine jet directed against the boundary. This aspect of the study could not be recorded by the high speed cameras (Robinson & Blake 1994).

4. Kelvin impulse

The Kelvin impulse, which was applied to bubble dynamics by Benjamin & Ellis (1966), provides a useful theoretical framework for interpreting the interaction of

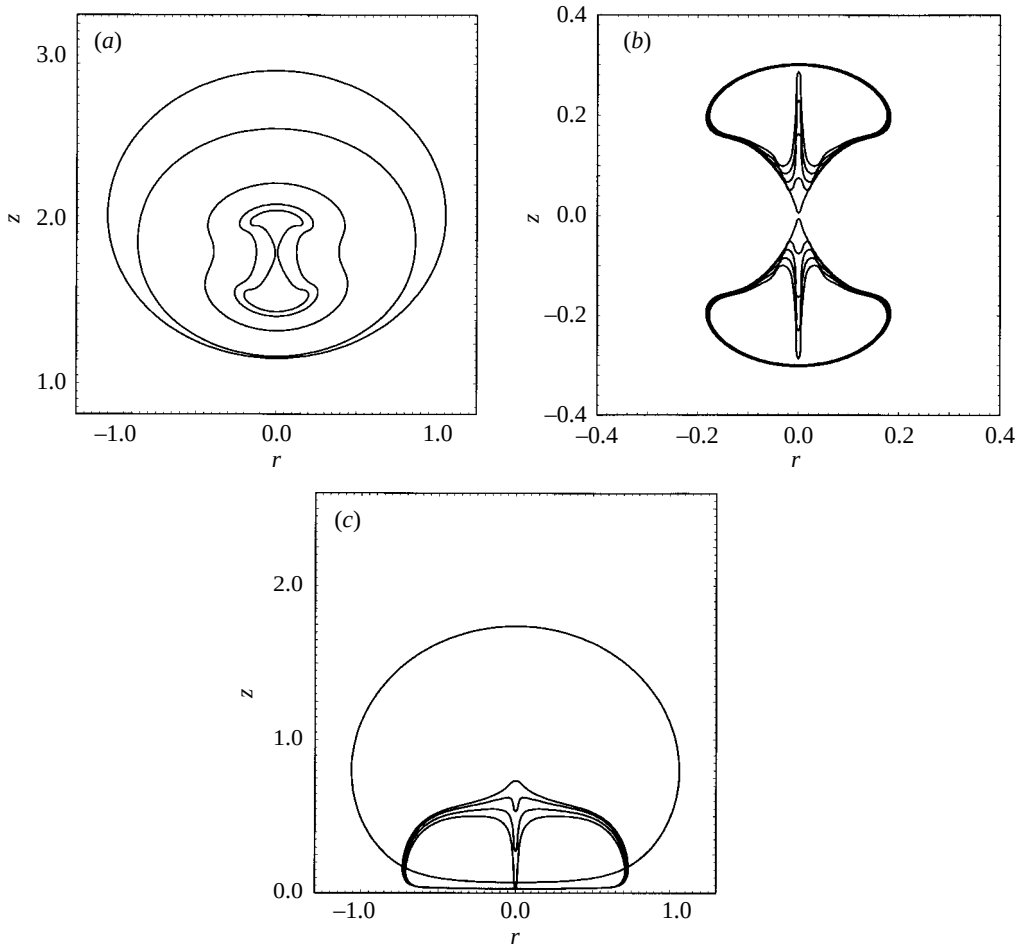

Figure 6. (*a*) Collapse of a vapour bubble in a stagnation point flow for $\gamma = 2.31$, $\beta = 0.126$. (*b*) The ultra high speed jets that form during the collapse of a perturbed spherical bubble after it divides into two. (*c*) Collapse of a vapour bubble in a stagnation point flow for $\gamma = 0.87$, $\beta = 0.09$.

a bubble with a rigid boundary, a free surface, or in a stagnation point flow. The Kelvin impulse (scaled by $R_{\mathrm{m}}^3(\rho\Delta p)^{1/2}$) is defined as

$$\boldsymbol{I} = \int_{S_{\mathrm{b}}} \phi \boldsymbol{n}\, \mathrm{d}S, \tag{4.1}$$

where S_{b} is the surface of the bubble. The rate of change of the Kelvin impulse can be written in terms of a force component $\boldsymbol{F}^{\Sigma}$ due to the Bjerknes effect of the boundary and a buoyancy force $\boldsymbol{F}^{g}$ (Blake & Cerone 1982),

$$\frac{\mathrm{d}\boldsymbol{I}}{\mathrm{d}t} = \boldsymbol{F}^{\Sigma} + \boldsymbol{F}^{g}. \tag{4.2}$$

where,

$$\boldsymbol{F}^{\Sigma} = -\int_{S_{\mathrm{b}}} \left\{ \frac{1}{2}|\nabla\phi|^2 \boldsymbol{n} - \frac{\partial\phi}{\partial n}\nabla\phi \right\} \mathrm{d}S, \tag{4.3}$$

and

$$\boldsymbol{F}^g = \delta^2 V \boldsymbol{e}_z, \tag{4.4}$$

$\boldsymbol{e}_z$ being a unit vector in the positive z-direction and V the bubble volume. These expressions can be derived (Newman 1977) by using the fact that the hydrodynamic force, $\boldsymbol{F}_\mathrm{h}$, on the bubble is zero, with

$$\boldsymbol{F}_\mathrm{h} = \int_{S_\mathrm{b}} p\boldsymbol{n}\,\mathrm{d}S = -\frac{\mathrm{d}\boldsymbol{I}}{\mathrm{d}t} - \int_{S_\mathrm{b}} \left\{\frac{1}{2}|\nabla\phi|^2\boldsymbol{n} - \frac{\partial\phi}{\partial n}\nabla\phi\right\}\mathrm{d}S + \delta^2 V\boldsymbol{e}_z. \tag{4.5}$$

The Kelvin impulse can be approximated using a multipole expansion for the potential due to the bubble and including the effects of any boundaries or ambient flow field (Blake 1988; Best & Blake 1994). It can then be used to predict the direction of bubble migration and jet penetration for a buoyant collapsing bubble near a rigid boundary or free surface in many cases, as indicated below.

In figure 7a, b, c computational predictions and experimental observations (free surface only) of the direction of final bubble migration and subsequent jet formation are shown for a range of values of the 'stand-off' parameter γ and the buoyancy parameter δ: in (a) for a rigid boundary (Best & Blake 1992); in (b) for a free surface (Blake *et al.* 1987); in (c) for a stagnation point flow where β corresponds to the dimensionless strength of the flow (Robinson & Blake 1994). In each of these cases there are opposing effects acting on the bubble motion: in (a) the upward buoyancy force opposes the downwards Bjerknes attraction towards the rigid boundary; in (b) the upward buoyancy force opposes the repulsive, downward directed, free surface Bjerknes force; and in (c) the 'effective buoyancy' term associated with the high stagnation pressure opposes the Bjerknes attraction towards the rigid boundary. The two curves in each of frames (a) and (c) of figure 7, correspond to two different methods used to calculate the null impulse line for the Kelvin impulse at the end of the first collapse: (i) a fixed spherical bubble model against (ii) a spherical bubble free to translate along the centreline. The key feature is the remarkable accuracy with which the simple idea of the Kelvin impulse can predict the direction of migration of nearly axisymmetric bubbles. However, when we move to the fully three-dimensional situation, the picture is not quite so promising. Figure 7d shows the bubble shapes for $\gamma = 1.2$, $\delta = 0.2$, $\alpha = 10$, $\lambda = 1.4$, while figure 7e gives the motion of the bubble centroid (continuous line) and the direction and magnitude of the Kelvin impulse. While there is some error in defining the actual jet tip, we find that variations between the jet direction and the Kelvin impulse vector can be as high as 10%. Further investigation of this aspect is being carried out (Blake & Tong 1995).

5. Acoustic cavitation

The irradiation of a liquid containing small bubbles by an acoustic field can result in the transformation of the low energy density of the acoustic waves into the very high energy density of the pulsating bubbles. When the wavelength of the acoustic pressure disturbance is much longer than the dimensions of the bubble, this phenomenon can be modelled using the formulation of the present discussion by defining the far field pressure in the liquid to be

$$p_\infty = p_\mathrm{h} + p_\mathrm{a}\cos\Omega t. \tag{5.1}$$

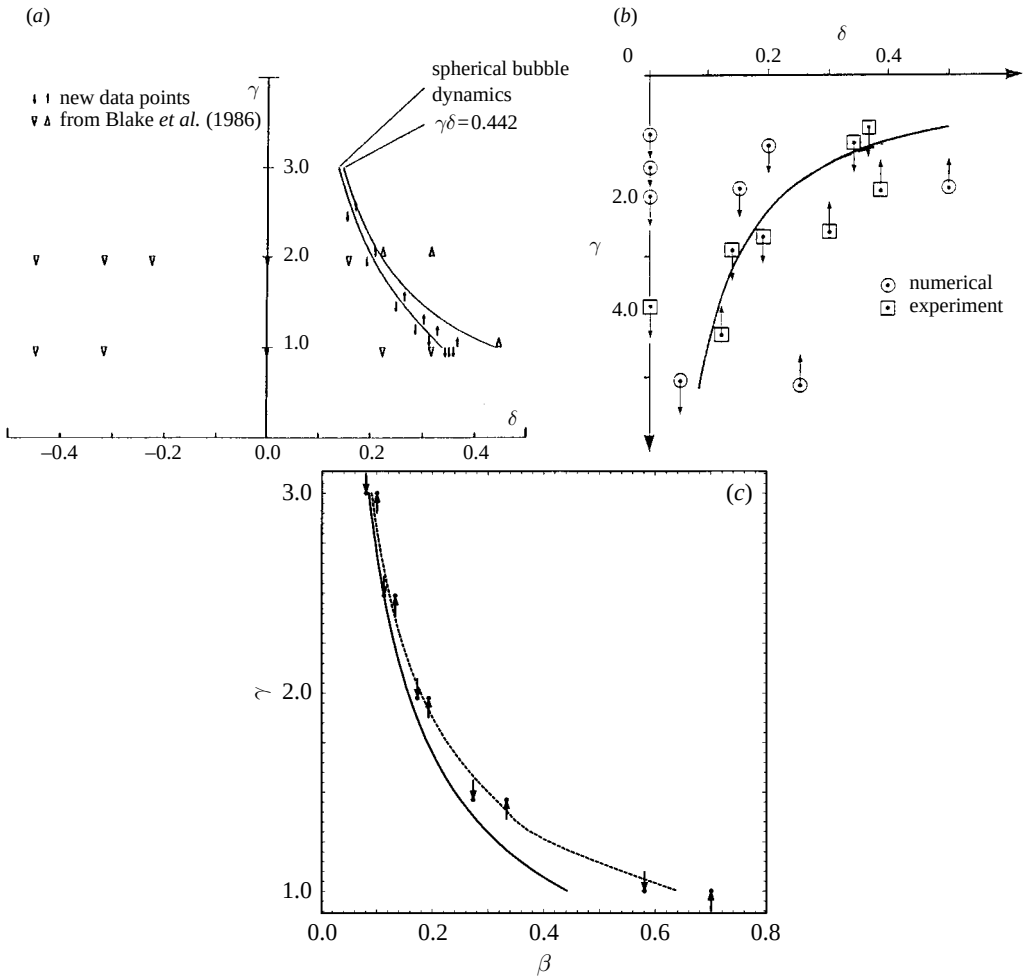

Figure 7. The null impulse curve for axisymmetric buoyant vapour bubbles ($\alpha = 0$): (*a*) above a rigid plane boundary (the direction of the arrow or triangle denotes the direction of jet formation computed by the boundary integral method); (*b*) beneath a free surface; (*c*) in a stagnation point flow, (—) fixed spherical bubble, (– –) translating spherical bubble.

Spherically symmetric pulsations in this context can be described by the Rayleigh–Plesset equation,

$$R\frac{\mathrm{d}^2R}{\mathrm{d}t^2} + \frac{3}{2}\left(\frac{\mathrm{d}R}{\mathrm{d}t}\right)^2 = \alpha\left(\frac{1}{R}\right)^{3\lambda} - \epsilon\cos\Omega t - 1 - \frac{2}{We}\frac{1}{R}, \tag{5.2}$$

where the pressure scale is now $\Delta p = p_\mathrm{h} - p_\mathrm{c}$ and the length scale is $R_\mathrm{m} = 2\sigma/\Delta p$ so that $\epsilon = p_\mathrm{a}/\Delta p$ with $\alpha = p_0/\Delta p$. This equation can be integrated numerically to any desired accuracy and it thus provides a useful comparison with the axisymmetric boundary integral computations of the same problem. The dynamic boundary condition for time stepping the bubble surface is modified to include the pulsating far field pressure:

$$\frac{\mathrm{d}\phi}{\mathrm{d}t} = \tfrac{1}{2}|\nabla\phi|^2 + 1 + \epsilon\cos\Omega t - \alpha\left(\frac{V_0}{V}\right)^{\lambda} + \frac{\kappa}{We}. \tag{5.3}$$

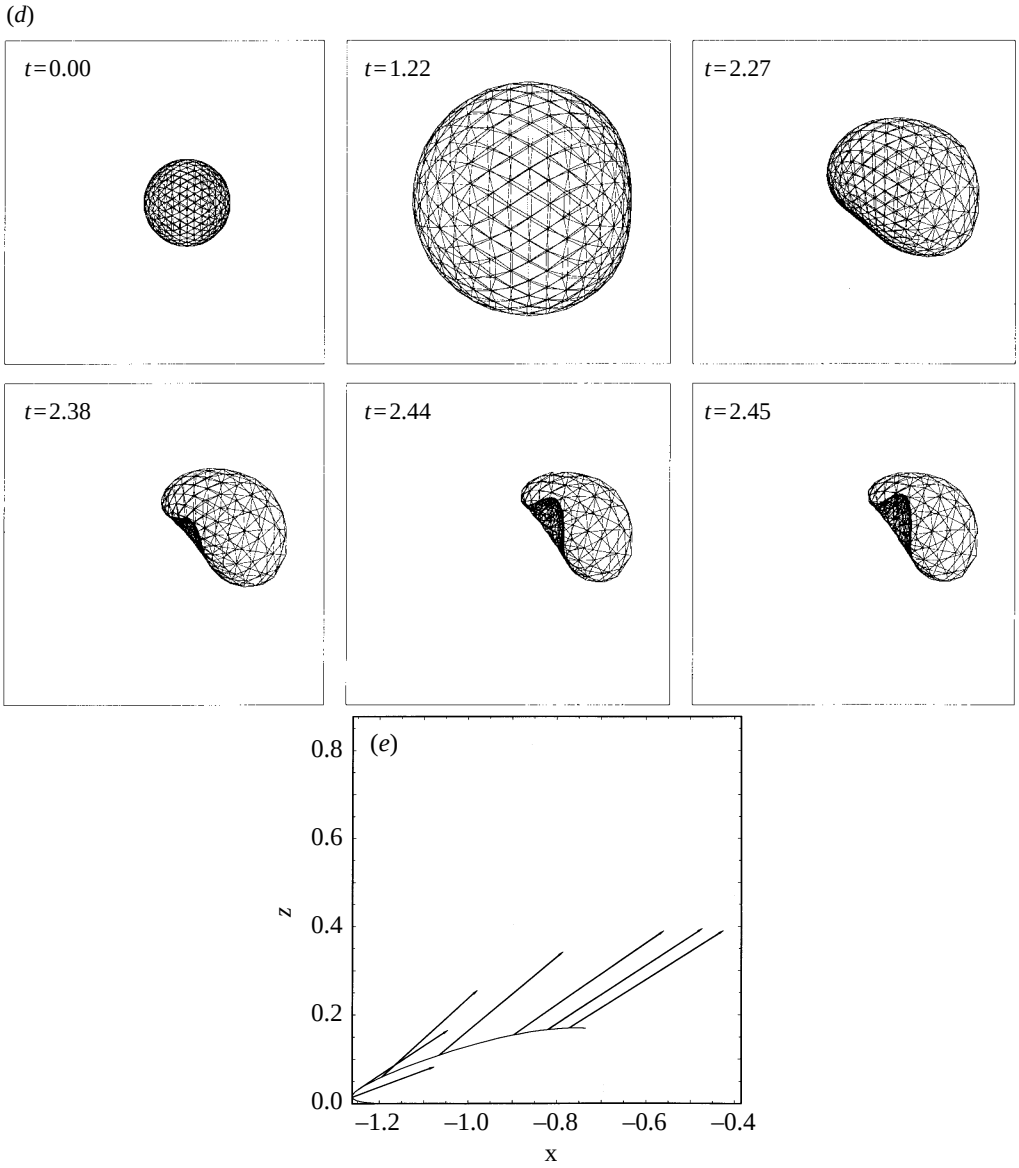

Figure 7. (*d*) Explosion bubble for $\gamma = 1.2$, $\delta = 0.2$, $\alpha = 10$, $\lambda = 1.4$. (*e*) The Kelvin impulse vectors for (*d*) related to the centroid motion (—).

In figure 8*a*, a comparison is made between the radius obtained from the Rayleigh–Plesset equation against that obtained from the volume of the axisymmetric bubble. The comparison up to $t = 30$ is excellent. However, if we plot out the bubble shape for $t > 30$ (figure 8*b*), it is observed that the bubble begins to develop an inward jet around the equator. This is probably due to a small numerical error developing with time in the code. Other studies where small non-dimensional perturbations of $O(10^{-4})$ are introduced and which use lower order spherical harmonics produce the expected characteristic shapes (Shaw 1994). Certainly experimental observations in Göttingen (Hentschel 1984) confirm that this behaviour can exist.

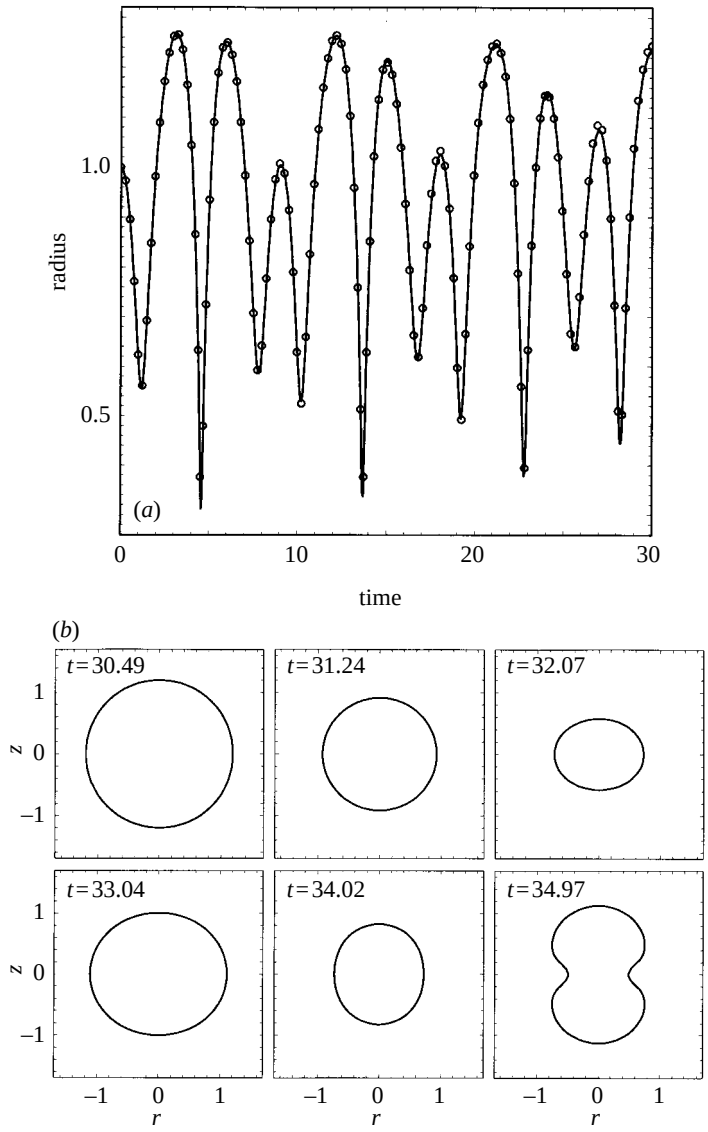

Figure 8. (a) Comparison between the radius-time curve calculated numerically by the boundary integral method (o) and the Rayleigh–Plesset equation (—). The corresponding parameters are given by $\Omega = 524$ kHz, $\Delta p = 1$ atm, $p_a = 0.333$ atm, $p_0 = 0.6$ atm and $We = 35$. (b) The bubble oscillations for $t > 30$, being the continuation of the boundary integral computation.

6. Conclusions

Considerable progress has been made over the last decade in our basic understanding of cavitation bubble collapse, the development of high speed liquid jets and the pressures associated with jet impact. Some of these developments are presented here. However, the theoretical studies to date are still highly idealized; either restricted to axisymmetric studies, or in rather special flow fields. Real problems often involve complicated flow behaviour (separation, tip vortices, turbulence) and three-dimensional geometries. However, the basic physical understanding that is beginning

to emerge from the simpler examples will provide insight into the more complicated real problems.

The research reported in this paper has been financially supported by the Australian Research Council, SERC, EPSRC and DRA Dunfermline and Fort Halstead.

References

Benjamin, T. B. & Ellis, A. T. 1966 The collapse of cavitation bubbles and the pressures thereby produced against solid boundaries. *Phil. Trans. R. Soc. Lond.* A **260**, 221–240.

Best, J. P. 1993 The formation of toroidal bubbles upon the collapse of transient cavities. *J. Fluid Mech.* **251**, 79–107.

Best, J. P. 1994 The rebound of a toroidal bubble. In *Proc. IUTAM Symp. on Bubble Dynamics and Interface Phenomena* (ed. J. R. Blake, J. M. Boulton-Stone & N. H. Thomas), pp. 405–412. Dordrecht: Kluwer.

Best, J. P. & Blake, J. R. 1992 Cavities, jets and toroidal bubbles. In *Proc. Ins. Mech. Engng, Camb.* C **453**, pp. 35–41.

Best, J. P. & Blake, J. R. 1994 An estimate of the Kelvin impulse of a transient cavity. *J. Fluid Mech.* **261**, 75–93.

Blake, J. R. 1988 The Kelvin impulse: application to cavitation bubble dynamics. *J. Austral. Math. Soc.* B **30**, 127–146.

Blake, J. R. & Cerone, P. 1982 A note on the impulse due to a vapour bubble near a rigid boundary. *J. Austral. Math. Soc.* B **23**, 383–393.

Blake, J. R. & Gibson, D. C. 1981 Growth and collapse of a vapour cavity near a free surface. *J. Fluid Mech.* **111**, 123–140.

Blake, J. R. & Gibson, D. C. 1987 Cavitation bubbles near boundaries. *A. Rev. Fluid Mech.* **19**, 99–123.

Blake, J. R. & Tong R. P. 1995 Jet impact in collapsing bubbles. In *Proc. 12th Aust. Fluid Mech. Conf., Sydney*, pp. 819–822.

Blake, J. R., Taib, B. B. & Doherty, G. 1986 Transient cavities near boundaries. 1. Rigid boundary. *J. Fluid Mech.* **170**, 479–497.

Blake, J. R., Taib, B. B. & Doherty, G. 1987 Transient cavities near boundaries. 2. Free surface. *J. Fluid Mech.* **181**, 197–212.

Blake, J. R., Boulton-Stone, J. M. & Tong, R. P. 1995 Boundary integral methods for rising, bursting and collapsing bubbles. In *B. E. applications in fluid mechanics* (ed. H. Power), pp. 31–71. Southampton: Computational Mechanics Publications.

Brennen, C. E. 1995 *Cavitation and bubble dynamics*. Oxford University Press.

Chahine, G. L. 1982 Experimental and asymptotic study of nonspherical bubble collapse. In *IUTAM Symp.: Mechanics and Physics of Bubbles* (ed. L. van Wijngaarden). Utrecht: Nijhoff.

Crum, L. A. 1995 Bubbles hotter than the sun. *New Scientist* **146**, 36–40.

Hentschel, W. 1984 Hochfrequenzholografie mit dem Argon-Ionen laser. *Optik* **68**, 283–310.

King, A. C. & Needham, D. J. 1994 The initial development of a jet caused by fluid, body and free-surface interaction. 1. A uniformly accelerating plate. *J. Fluid Mech.* **268**, 89–101.

Knapp, R. T. 1955 Recent investigations of the mechanics of cavitation and cavitation damage. *Trans. ASME* **77**, 1045–1054.

Longuet-Higgins, M. S. 1983 Bubbles, breaking waves and hyperbolic jets at a free surface. *J. Fluid Mech.* **127**, 103–124.

Longuet-Higgins, M. S. & Cokelet, E. D. 1976 The deformation of steep surface waves on water, I. A numerical method of computation. *Proc. Roy. Soc. Lond.* A **350**, 1–26.

Moss, W. C., Clarke, D. B., White, J. W. & Young, D. A. 1994 Hydrodynamic simulations of bubble collapse and picosecond sonoluminescence. *Phys. Fluids* **6**, 2979–2985.

Newman, J. N. 1977 *Marine hydrodynamics*. Cambridge, MA: MIT Press.

Oğuz, H. N. & Prosperetti, A. 1990 Bubble entrainment by the impact of drops on liquid surfaces. *J. Fluid Mech.* **219**, 143–179.

Robinson, P. B. & Blake, J. R. 1994 Dynamics of cavitation bubble interactions. In *Proc. IUTAM Symp. on Bubble dynamics and Interface Phenomena* (ed. J. R. Blake, J. M. Boulton-Stone & N. H. Thomas), pp. 55–64. Dordrecht: Kluwer.

Shaw, S. J. 1994 Surface mode deformations on an oscillating bubble. In *Proc. IUTAM Symp. on Bubble Dynamics and Interface Phenomena* (ed. J. R. Blake, J. M. Boulton-Stone & N. H. Thomas), pp. 355–363. Dordrecht: Kluwer.

Starrett, J. E. 1982 Bubble dynamics in stagnation flow. Ph.D. thesis, University of California, San Diego.

Zhang, S., Duncan, J. H. & Chahine, G. L. 1993 The final stage of the collapse of a cavitation bubble near a rigid wall. *J. Fluid Mech.* **257**, 147–181.